IEEE Access
Multidisciplinary | Rapid Review | Open Access Journal

Received May 29, 2020, accepted July 1, 2020, date of publication July 7, 2020, date of current version July 17, 2020.

Digital Object Identifier 10.1109/ACCESS.2020.3007705

Correction of Atmospheric Model Through Data Mining With Historical Data of Two-Line Element

XUE BAI[1], CHUAN LIAO[2], MING XU[1], AND YARU ZHENG[1]
[1]School of Astronautics, Beihang University, Beijing 100191, China
[2]No. 10 Research Institute, China Electronics Technology Group Corporation, Chengdu 610036, China

Corresponding author: Ming Xu (xuming@buaa.edu.cn)

This work of Ming Xu was supported in part by the National Natural Science Foundation of China under Grant 11772024 and Grant 11432001.

ABSTRACT The existing atmospheric mass density models (AMDM) would produce considerable errors in orbital prediction for Low Earth Orbit (LEO) satellites. In order to reduce these errors and correct the AMDM, this paper presents methods based on data mining with historical data of two-line element (TLE). Starting from a typical LEO satellite, TIANHUI, two orbital dynamical models are firstly proposed as the simulation environment to generate training data. The historical TLE data are regarded as actual space environment and used to generate application data. Secondly, three data mining methods, Random Forest (RF), Artificial Neural Network (ANN) and Support Vector Machine (SVM), are combined with the training data to investigate their feasibility in recovering the known deviation of AMDM under simulation environment. Training results show that RF displays the best performance and achieves the accuracy of 99.99%, while the other two methods only achieve 86.83% and 71.90% respectively. Thirdly, under the actual space environment, this paper uses new training and application data to research the ability of the three methods in recovering the unknown deviation of the AMDM and improve the accuracy of orbital prediction. Numerical results are evidential to the accuracy of the proposed methods based on data mining. It is concluded that the capabilities of the data mining for correction for the atmospheric model are very promising, with great potential to advance practical applications on on-orbit propagation.

INDEX TERMS Data mining, atmospheric mass density model, random forest, artificial neural network, support vector machine, two-line element.

I. INTRODUCTION

Data mining, also known as Knowledge Discovery in Database (KDD), was first emerged in the 1980s and got rapid development in the 1990s. It provides a method to discover the potential pattern in a big database. Feasibility, usefulness, validity and scalability are the four major problems in this technology [1]. In the past few years, some industries and researchers have applied KDD to improve their services and products. The financial securities industry use KDD to predict the fluctuation and tendency to share price, and analyze the investment habit of investors [2]. Fu [3] gave a comprehensive revision on the existing time series data mining research which is categorized into representation and indexing, similarity measure, segmentation, visualization, and mining. He thought that according to the unique behavior of the time series data, existing research is still inadequate. Bianchi *et al.* [4] proposed a framework for identifying patterns and regularities in the pseudo-anonymized Call Data Records. Their work could be employed by telecommunication companies for monitoring and understanding the behaviors of their subscribers. Pillay *et al.* [5] presented a special issue about automatic design of machine learning and search algorithms. Many novel ideas and insights based on KDD are also provided for complex networks [6]. Li *et al.* [7] took uses of both and local and global topological properties to enhance the performance of big data network computation. They also proposed efficient algorithm with fast convergence for sparse networks [8].

Some researchers have done a lot of work on artificial intelligence and data mining applied in traditional aerospace engineering. From the perspective of the database, Chen *et al.* [9] gave an overview of data mining by investigating various new data mining technologies, including the Apriori algorithm, multiple-level association rule, classification based on decision trees, etc. Tanner *et al* [10] presented the concept

The associate editor coordinating the review of this manuscript and approving it for publication was Huiling Chen.

of onboard data mining and believed that large networks of remote sensors would be becoming more common in improving technology and declining costs. Immediate management of the collected data on board would contribute to increasing the network communication capabilities and cutting down expenses. Sánchez Sánchez *et al.* [11] used Deep Neural Network (DNN) to solve the Hamilton-Jacobi-Belman equation and provided a near-optimal control strategy for spacecraft. Hennes *et al.* [12] focused on the problem of optimally transferring a spacecraft from an original asteroid to the targeted one and studied in detailed approximations for the phasing value, the maximum initial mass and the arrival mass. Li *et al.* [13] analyzed the connotation and extension of Spatial Data Mining and Knowledge Discovery (SDMKD), and used it to reveal potential patterns from space databases automatically or semi-automatically. Gong *et al.* [14] focused on the lack of effective technologies of data mining for volume remote sensing data and designed a technological framework of the remote sensing data mining and knowledge discovering system. Peng and Bai [15] concentrated on the lack of area-to-mass ratio of a resident space object in most space catalogs and proposed an improved method of satellite orbital prediction. They used Random Forest (RF) to learn the connection between the consistency error and area-to-mass ratio, and Support Vector Machine (SVM) to learn the errors of orbital prediction [16], [17]. However, their work is just based on their simulation environment and did not apply TLE data or any other actual on-orbit data. Hu *et al.* [18] analyzed the working and fault characteristic of liquid–propellant rocket engine, and used data mining techniques to detect and diagnose the fault of liquid-propellant rocket engines. However, they did not use any actual data either. In order to rapidly diagnose the satellite's fault, Xu and Pi [19] proposed a method to mine abnormal patterns in satellites based on Prefix Span. With the same purpose, Zhao and Li [20] proposed a new fault diagnosis method of spacecraft based on time series data mining. We have also used data mining techniques to detect the orbital maneuvers of satellites at different scales in a previous study [21].

North American Air Defense Command (NOARD) has accumulated a large amount of historical TLE data of the LEO satellite. TLE data are ''mean'' values obtained by removing periodic variations in a particular way. Therefore, they are using an obsolete true equator and mean equinox (TEME) coordinate system. To predict satellite position and velocity under the inertial coordinate system, NOARD has released the simplified general perturbations (SGP4) propagator to reconstruct periodic variations [22]. It is noticeable that the derived orbital elements are fundamentally decided by the accuracy of original TLE data. The TLE uncertainties are originated from semi-analytic SGP4 orbit model for orbit propagation, radar tracking and processing. For LEO satellites, the TLE data within 5-day propagation provide appropriately accurate orbital information with errors remaining bounded within roughly 0.5 km [23], [24]. In this paper, the TLE data and SGP4 are used to calculate the satellite's historical on-orbit states.

The satellites would be influenced by various effects of perturbations, including Earth's gravity, third-body perturbation, solar radiation pressure and atmosphere drag, etc. Especially for LEO satellites, atmosphere drag would cause considerable orbit decay and it is the main error source in orbital prediction. Most empirical atmospheric density models [25], such as Jacchia [26], NRLMSISE [27], DTM [28], Jacchia–Bowman 2006/2008 [29], [30] and Russian GOST [31] combine theoretical computation with drag measurements of satellites. Their accuracy is much better than the traditional exponential one, but still no better than 10%∼30%. It is worth mentioning that indirect solar activity has a great influence on AMDM by thermosphere and causes cycle, seasonal and geomagnetic effects, which result in errors [32]. Generally, there are two main methods to increase the accuracy of atmospheric density model [33]. One is to derive the AMDM directly using measurements from a high-accuracy onboard accelerometer [34]. The other is to calibrate the AMDM using large numbers of orbital measurements with lower accuracy [35]. Chen *et al* studied the performance of the AMDM coefficient calibration method, the Nazarenko method, and the parameterization method in improving orbital prediction of LEO objects [36]. The central idea of this paper is to use the second method based on historical TLE data to correct the AMDM and realize the orbital prediction. Meanwhile, data mining technology is good at dealing with a large amount of data to excavate those hidden, short-term but potentially useful, providing new techniques to improve the accuracy of the AMDM instead of replacing them and benefit the orbital prediction of LEO satellite.

Based on the historical TLE data of TIANHUI satellite, this paper investigates the feasibility of data mining technology in recovering the deviation of the existing AMDM. Two orbital dynamical models, the accurate model and the simplified one with deviation, are built as the simulation environment of TIANHUI to verify the feasibility of data mining technology. The historical TLE data are used as application data to correct the atmosphere model errors. Three data mining methods, including RF, ANN and SVM, are used to classify and correct the AMDM in orbital prediction. This paper is mainly carried out from two aspects: methodology and practical application, shown as the flowchart in Figure 1. In the stage of methodology, the differences between the accurate model and the simplified one with known deviation generate the training and application data. The three data mining methods learn on the training data to obtain three classifiers and then apply them on the application data to get model errors. The training results verify the feasibility of data mining technology in correcting AMDM errors. In the stage of practical application, the application data are generated from the differences of the accurate model and historical TLE data with unknown errors. After retraining with training data, the classifiers import the application data to recover the real AMDM errors. The errors

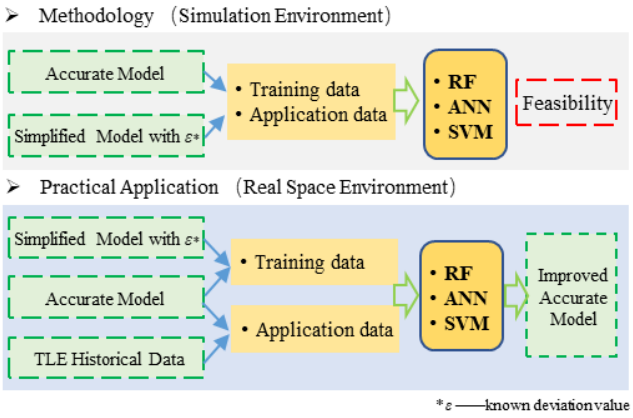

FIGURE 1. Flowchart of the data mining methods in this paper: in the stage of methodology, the data are generated from the differences between accurate model and the simplified one with known deviation and then are trained to obtain three classifiers; in the stage of practical application, the application data are generated from the differences of accurate model and historical TLE data and the classifiers import the application data to recover the real AMDM errors.

are then added to the accurate AMDM to get the improved accurate model which exactly indicates the correction results.

We make four contributions in this paper listed as following: 1) It is proved that data mining provides a practical technique to refine valuable information of orbital elements as well as atmospheric density model from historical TLE data. 2) The feasibility of data mining in predicting the AMDM errors is verified in simulation environment provided by the accurate orbital dynamical model and the simplified model with deviation. 3) The proposed methods are demonstrated to have a good performance on recovering the unknown deviation of the AMDM through application data derived from historical TLE data. 4) Orbital prediction is promoted by the improved accurate model with error correction of the classification methods according to the numerical results. Furthermore, data mining methods are verified that with the accessible data based on the point-to-point historical TLE data, they can provide an accurate calculation of satellite's on-orbit state for ground station and design of satellite's maintenance control, which are important for orbital prediction.

II. BASIC KNOWLEDGE

A. ORBIT DYNAMICS

Accurate orbital prediction needs accurate modeling of the space environment. According to Reference [37], Table 1 gives an overview of the magnitude of the major perturbations. It deals with a LEO satellite with an orbital altitude of 500 km. The absolute values of acceleration are computed as mean values over the time interval of the integration of one day. In order of importance, Earth's gravity, solid Earth tides, solar attraction perturbation, solar radiation pressure and atmospheric drag are taken into consideration in the following orbit dynamics. Due to other perturbations, such as direct radiation pressure and connected relativistic factors, in small orders of magnitude compared with the TLE data errors themselves, they are not included in the accurate orbit

TABLE 1. Accelerations acting on LEO with an orbital altitude of 500 km.

Perturbation	Acceleration (m/s^2)
$\frac{1}{r^2}$-Term	8.42
Oblateness	1.5×10^{-2}
Atmospheric Drag	7.9×10^{-7}
Higher Terms of the Earth's Gravity Field	2.5×10^{-4}
Solar Attraction	5.0×10^{-7}
Direct Radiation Pressure	9.7×10^{-8}
Solid Earth Tides	1.1×10^{-7}

dynamic and not listed in the following contents. The long-term perturbation, such as 11-year solar activity, is regarded as constant because of the short-term TLE data used in this paper.

This section presents the mathematical models of each perturbation above. According to Reference [38], Earth gravitational potential can be written as the following form:

$$U = \frac{GM_e}{R_e}\sum_{n=0}^{\infty}\sum_{m=0}^{n}(C_{nm}V_{nm} + S_{nm}W_{nm}) \tag{1}$$

where

$$V_{nm} = \left(\frac{R_e}{r}\right)^{n+1} P_{nm}(\sin\varphi)\cos m\lambda$$
$$W_{nm} = \left(\frac{R_e}{r}\right)^{n+1} P_{nm}(\sin\varphi)\sin m\lambda, \tag{2}$$

GM_e is the Earth gravitational constant, r is the distance from the Earth's center, φ is the geocentric latitude and λ is the longitude of the satellite, R_e is the equatorial radius of the Earth, P_{nm} is the associated Legendre polynomial of degree n and order m, C_{nm} and S_{nm} are the coefficients which describe the dependence on the Earth's internal mass distribution. Besides, this paper uses EGM96 model. The detailed values can be found in Reference [39].

Therefore, the acceleration $\ddot{\boldsymbol{r}}$ in the Earth-center fixed coordinate system can be calculated by V_{nm} and W_{nm} listed in Equation (2) as

$$\ddot{x} = \sum_{n,m}\ddot{x}_{nm} \quad \ddot{y} = \sum_{n,m}\ddot{y}_{nm} \quad \ddot{z} = \sum_{n,m}\ddot{z}_{nm} \tag{3}$$

where

$$\ddot{x}_{nm} = \begin{cases} \frac{GM_e}{R_e^2}\left(-C_{n0}V_{n+1,1}\right) & m = 0 \\ \frac{GM_e}{2R_e^2}\left[-\left(C_{nm}V_{n+1,m+1} + S_{nm}W_{n+1,m+1}\right) + \frac{(n-m+2)!}{(n-m)!}\left(C_{nm}V_{n+1,m-1} + S_{nm}W_{n+1,m-1}\right)\right] & m > 0 \end{cases}$$

$$\ddot{y}_{nm} = \begin{cases} \frac{GM_e}{R_e^2}\left(-C_{n0}W_{n+1,1}\right) & m = 0 \\ \frac{GM_e}{2R_e^2}\left[-\left(C_{nm}W_{n+1,m+1} + S_{nm}V_{n+1,m+1}\right) + \frac{(n-m+2)!}{(n-m)!}\left(-C_{nm}V_{n+1,m-1} + S_{nm}W_{n+1,m-1}\right)\right] & m > 0 \end{cases}$$

$$\ddot{z}_{nm} = \frac{GM_e}{R_e^2}\left[(n-m+1)\left(-C_{nm}V_{n+1,m} - S_{nm}W_{n+1,m}\right)\right]$$

In accordance with the acceleration $\ddot{\boldsymbol{r}}$ obtained from Equation (3), all the perturbation accelerations in the following are also transferred to the Earth-center fixed coordinate system. Equation (4) shows the transfer method from other coordinate systems to Earth-center fixed coordinate system:

$$\begin{aligned} \boldsymbol{r}_e &= \boldsymbol{U}(t)\,\boldsymbol{r}_s \\ \ddot{\boldsymbol{r}}_e &= \ddot{\boldsymbol{U}}(t)\,\boldsymbol{r}_s + 2\dot{\boldsymbol{U}}(t)\,\dot{\boldsymbol{r}}_s + \boldsymbol{U}(t)\,\ddot{\boldsymbol{r}}_s \end{aligned} \tag{4}$$

where $\boldsymbol{U}(t)$ is a time-dependent matrix that describes the Earth's rotation. Furthermore, the rigorous calculation of $\boldsymbol{U}(t)$ has to account for the long and short-term perturbations of the Earth's axis, known as precession and nutation, which is based on IAU1980 standards [38].

The perturbation effects of solid Earth tides imposed by the Sun or the Moon can be transformed into the time-dependent corrections of the geopotential coefficients. Besides, ocean tide potential can be expanded in terms of spherical harmonics and mapped to geopotential coefficients through the following equation:

$$\begin{Bmatrix}\Delta C_{nm}\\ \Delta S_{nm}\end{Bmatrix} = \frac{4\pi G R_e^2 \rho_w}{GM_e}\frac{1+k'_n}{2n+1} \times \begin{Bmatrix}\sum\limits_{s(n,m)}\left(C^+_{snm}+C^-_{snm}\right)\cos\theta_s + \left(S^+_{snm}+S^-_{snm}\right)\sin\theta_s \\ \sum\limits_{s(n,m)}\left(S^+_{snm}+S^-_{snm}\right)\cos\theta_s - \left(C^+_{snm}+C^-_{snm}\right)\sin\theta_s\end{Bmatrix} \tag{5}$$

where ρ_w is the density of the seawater, k'_n is the load-deformation coefficients, $C^{\pm}_{snm}$ and $S^{\pm}_{snm}$ are the ocean tide coefficients in meters for the tide constituent, θ_s is the weighted sum of the six Doodson variables which denote fundamental arguments of the Sun's and Moon's orbit.

The acceleration $\ddot{\boldsymbol{r}}_i$ caused by the Sun's gravity in the inertial coordinate system is

$$\ddot{\boldsymbol{r}}_i = \frac{GM\,(\boldsymbol{s}-\boldsymbol{r}_i)}{|\boldsymbol{s}-\boldsymbol{r}_i|^3} - \frac{GM\boldsymbol{s}}{|\boldsymbol{s}|^3} \tag{6}$$

where $\boldsymbol{r}_i$ and $\boldsymbol{s}$ are the position vectors of the satellite and Sun, respectively, and M is the mass of Sun.

The acceleration $\ddot{\boldsymbol{r}}_j$ caused by solar radiation pressure in the inertial coordinate system is

$$\ddot{\boldsymbol{r}}_j = -P_s\frac{1AU^2}{r_s^2}\frac{A}{m}\cos(\theta)[(1-\varepsilon)\boldsymbol{e}_s + 2\varepsilon_r\cos(\theta)\boldsymbol{n}] \tag{7}$$

where P_s is the solar radiation pressure, AU is the astronomical unit, r_s is the magnitude of the geocentric position vector of Sun, $\boldsymbol{n}$ is the normal unit vector of the surface A, $\boldsymbol{e}_s$ is the unit vector pointing to the direction of Sun, θ is the angle between the vector $\boldsymbol{n}$ and the vector $\boldsymbol{e}_s$, ε_r is the reflectivity coefficient of the material used by the satellite. Besides, because of the Earth's partial and full eclipse, this paper uses the eclipse prediction algorithm from Reference [40] to predict the eclipse events.

Atmosphere drag is the major non-conservative force for the LEO satellite. The acceleration $\ddot{\boldsymbol{r}}_a$ caused by the atmosphere in the inertial coordinate system is

$$\ddot{\boldsymbol{r}}_a = -\frac{1}{2}C_D\frac{A}{m}\rho v_r^2\boldsymbol{e}_v \tag{8}$$

where C_D is the drag coefficient, A is the windward area, m is mass of the satellite, ρ is the atmospheric density at the position of the satellite, v_r is the velocity relative to the atmosphere and e_v is the unit vector of relative velocity, i.e. $\boldsymbol{e}_r = \boldsymbol{v}_r/|\boldsymbol{v}_r|$. It can be seen that the parameters in Equation (8) except v_r can cause certain errors and they are required to refine through the correction derived from the data mining technique. MSISE-86 atmospheric density model, the most common model, is applied to calculate the atmospheric density ρ. The traditional modeled atmospheric density can predict long-term behaviors just from the physical factors, but on the other hand, it is weak in refining more accurate short-term predictions [41]. In the latter case, some historical data can contribute to refining the short-term prediction, which is reported in this paper. The proposed data mining technique can excavate those hidden, short-term but potentially useful information from the historical TLE data.

What's more, from the point of mission design, there are a lot of other complicated noise sources during the process of state transformation, such as the attitude and orbit control, guidance system and transform in the reference frames, which have developed algorithms to deal with the noise in published references. Thus, these noises are not the points discussed in this paper.

B. ACCURATE MODEL AND SIMPLIFIED MODEL WITH DEVIATION

Section II.A gives the accurate mathematical models of each perturbation in space. These models provide the basic data in orbit prediction of the satellite. In order to generate training and application data for classifiers, this section gives two orbital dynamical models: the accurate model which is the reference of orbit prediction and simulates an ''actual'' space environment, and the simplified one with deviation which uses simplified mathematical models and adds known deviation value ε to the AMDM. From the perspective of engineering, the product of parameters $C_D\frac{A}{m}\rho$ in Equation (8) causes certain errors and is usually regarded as one parameter C_s during satellite design. Therefore, the goal of this paper is to correct C_s. As a result, Equation (8) has been changed in the simplified model with deviation ε to the following form:

$$\ddot{\boldsymbol{r}}_a = -\frac{1}{2}(1+\varepsilon)\,C_D\frac{A}{m}\rho v_r^2\boldsymbol{e}_v = -\frac{1}{2}(1+\varepsilon)\,C_S v_r^2\boldsymbol{e}_v \tag{9}$$

The orbit data are generated by these two models and the differences between them are regarded as training data. Specific parameter settings are shown in Table 2. The accuracy of the models with these perturbations here is enough to use as the training data because the errors predicted by these models are beneficial for convergence of the classification and make it easy to get the classifiers.

TABLE 2. Parameter setting of two models.

Model	Accurate Model	Simplified Model with Deviation
Earth Shape	WGS84	WGS84
Gravity Field	70×70	5×5
Third-body Perturbation	Sun	~
Solar Radiation Pressure	Accurate Eclipse Prediction	~
Atmospheric Model	MSISE-86	MSISE-86×(1+ε)

Here the orbital states derived from point-to-point TLE data are regarded as the near-real ones. Compared with them, both the accurate model and the simplified one cause certain errors Δ_{at} and Δ_{sa} in orbital prediction, as shown in Figure 2. It uncovers that the accurate model contains an unknown deviation value ε_a of the AMDM. Meanwhile, the simplified model with deviation contains known deviation value ε_s which is added to the AMDM artificially. The purpose of this paper is to recover the deviation value ε of the AMDM to reduce the certain errors Δ in orbital prediction and taking these results to improve orbital prediction.

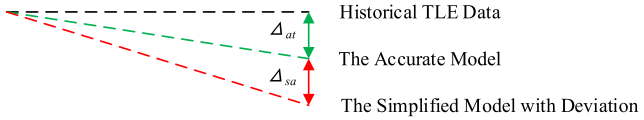

FIGURE 2. Errors caused by different dynamical models: compared with the historical TLE data, the accurate model and the simplified one have certain errors in orbital prediction.

C. DATA MINING METHODS

Data mining techniques can extract valuable information from volume disordered data. But the process is relatively complicated. Considering the characteristics of the research content and data in this paper, this section introduces three typical classification methods used to deal with orbit data and meanwhile validates their accuracy.

RF is a popular algorithm that combines multiple trees through a certain bridge. Figure 3 shows the visualization of a random forest model making a prediction. RF chooses n instances from all instances and m classes from all classes, randomly. It concludes the best partition properties to build Decision Tree (DT). It consists of a large number of individual DTs that operate as an ensemble. After repeating the above procedures m times, m trees could be obtained and each tree in the random forest represents a class prediction. Through voting mechanism, the class with the most votes becomes the final prediction.

Here are three major advantages of RF: 1) as for multiple data, RF can generate highly accurate classifier; 2) RF can internally generate the unbiased estimation for the errors after generalization while building the forest; 3) RF can evaluate the importance of the variables while determining the final class.

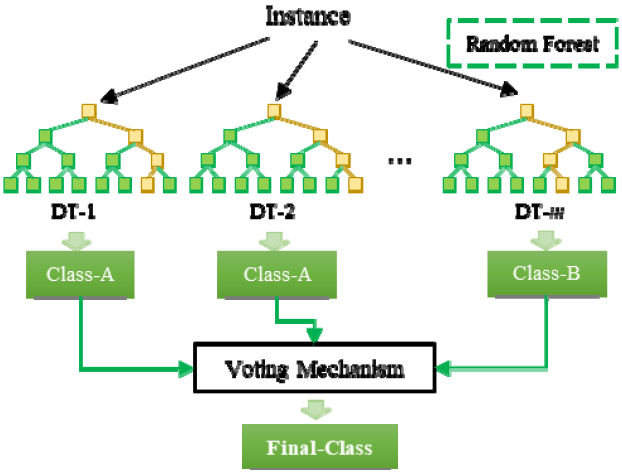

FIGURE 3. Sketch map of random forest: the main processes are DTs building and voting mechanism.

ANN is a mathematical model similar to the structure of synaptic connection in the human brain. From an early viewpoint, the human brain is made up of nerve cells named ''Neuron'' which are connected through axon and dendrite. Similarly, ANN is made up of a group of nodes and directed chains. Figure 4 plots the sketch map of ANN Perceptron, where the perceptron is the simplest model of ANN, including multiple input nodes and one output node. These nodes are ''Neuron'' in ANN. Each input node is connected to the output node through a weighted chain. These weighted chains are ''Synapse'' in ANN. Same as the human brain, training a perceptron is to change the weight constantly till the perceptron could fit the connection of the input and the output.

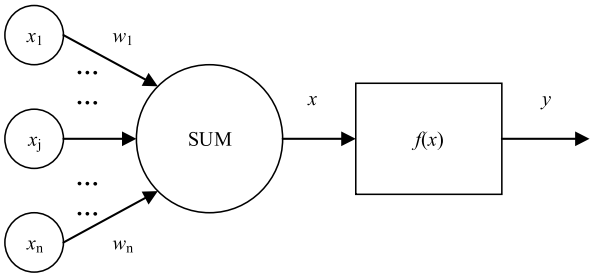

FIGURE 4. Sketch Map of ANN Perceptron.

This paper applies a feed-forward backpropagation network in orbital prediction. Feedforward represents that the neurons in each layer are only connected to the previous layer and output to the next layer, there is no feedback between the layers, and no adjustment is made to the parameters of the network. Backpropagation means that the error will be propagated back to adjust the weight and threshold. Backpropagation is a conventional training method for the feed-forward neural network during which the neurons adapt their weights to acquire new knowledge. A multi-layer neural network,

TABLE 3. Comparison of different kernel functions.

Kernel function	Accuracy
Quadratic	71.90%
Cubic	53.20%
Gaussian	50.70%
Linear	Fail

which has at least one hidden layer, could fit any target functions theoretically. However, ANN is much sensitive to noise and relatively time-consuming.

SVM is based on statistical learning theory, and the original intention of SVM is to build a hyperplane to segment multi-classes. Figure 5 is the sketch map of SVM. It shows that during its building process, SVM would try to maximize the interval between multi-classes.

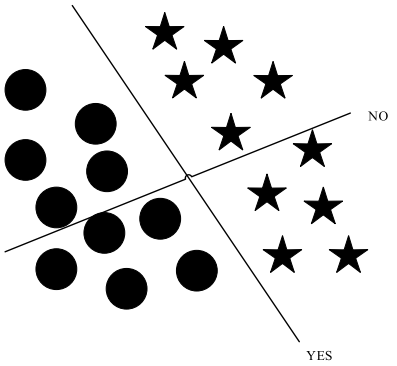

FIGURE 5. Classification algorithm of SVM: the circles and pentagrams are divided by SVM.

There are three key points in SVM as max interval, kernel function and Lagrange dual theory. This paper uses rational quadratic kernel, which is a kind of radial basis function, as the kernel function after trying different kernel functions and it can be written as

$$k(\boldsymbol{x}, \boldsymbol{y}) = 1 - \frac{\|\boldsymbol{x} - \boldsymbol{y}\|^2}{\|\boldsymbol{x} - \boldsymbol{y}\|^2 + c}. \tag{10}$$

where $k(\cdot, \cdot)$ denotes the kernel function, $\boldsymbol{x}$, $\boldsymbol{y}$ are sample data vectors and c is a constant. The rational quadratic kernel appears as a substitute for the Gaussian kernel, which has a better anti-interference ability for noise in the data, with less time consumption meanwhile. Besides, the comparison of different kernel functions is tabulated in Table 3 using the training data and accuracy definition from Section III.

III. CLASSIFIER TRAINING AND EVALUATION

In this section of methodology, the two orbital dynamical models in Section II are used to conduct orbital prediction and generate training data starting from the same specific epoch. The accurate model gives a high-order description of the space environment with the perturbations and provides an environment without observation and measurement errors compared with TLE data. As for real application in the satellite control center, the low-order model is usually used to propagate the orbital information due to the existing initial errors. Although the processing procedure in this section is based on simulation, the data accuracy is ensured, higher than other observation data. So, in this simulation environment, the accurate model is assumed as the ''actual'' space condition and the simplified model is served to predict and propagate. It is meaningful and practical. Then the data are imported to the three classification methods. After setting proper parameters, three classifiers can be obtained and then their performance is compared.

TIANHUI is a Chinese remote sensing satellite that is successfully launched on August 24th, 2010. Its orbital altitude is around 500 km and atmosphere drag would cause considerable orbital decay. Therefore, this section chooses the real on-orbit state of this satellite as the starting point of orbital prediction.

A. GENERATION OF TRAINING DATA AND PARAMETER SETTING

All the simulations are implemented by Matlab2017a on a PC with Intel® CORE i5-4590 processor and 8G RAM. The starting epoch of simulation is set at 21:07:05, May 31st, 2016 (UTC). The real on-orbit state of this satellite at the starting epoch is shown in Table 4, where a is semi-major axis, e is eccentricity, i is orbit inclination, Ω is the right ascension of ascending node, ω is the argument of perigee, M is mean anomaly, $\boldsymbol{r} = [r_x, r_y, r_z]$ is the satellite position vector in inertial coordinate system, $\boldsymbol{v} = [v_x, v_y, v_z]$ is the satellite velocity vector in inertial coordinate system.

TABLE 4. Initial states of simulation.

a (km)	e	i (°)	Ω (°)	ω(°)	M (°)
6871.2093	0.0025	97.5604	285.7813	95.2957	21.1683
r_x (km)	r_y (km)	r_z (km)	v_x (km/s)	v_y (km/s)	v_z (km/s)
-1611.4252	2731.7174	6081.6417	-1.4261	6.6905	-3.3722

The sample interval between two adjacent TLE data points of TIANHUI is less than 1 day. Since the TLE propagation accuracy is with respect to the propagation intervals and a five-day or less propagation is likely used [23], the propagation intervals in this paper are set as following: the minimal propagation interval is 10s and the maximal propagation time is 1 day. Each discrete point is corresponding to one on-orbit state $\boldsymbol{X}_j$ after integer prediction interval which is made up of 25 variables, as (11), as shown at the bottom of the page, where Δt_j is the prediction interval of this point, Δ means

$$\boldsymbol{X}_j = \begin{bmatrix} \Delta t_j & a_j & e_j & i_j & \Omega_j & \omega_j & M_j & r_{x_j} & r_{y_j} & r_{z_j} & v_{x_j} & v_{y_j} & v_{z_j} \\ & \Delta a_j & \Delta e_j & \Delta i_j & \Delta\Omega_j & \Delta\omega_j & \Delta M_j & \Delta r_{x_j} & \Delta r_{y_j} & \Delta r_{z_j} & \Delta v_{x_j} & \Delta v_{y_j} & \Delta v_{z_j} \end{bmatrix} \tag{11}$$

the differences between the simplified model with deviation and the accurate model, and the subscript j means the ordinal of this state. In conclusion, 181440 pairs of satellite on-orbit states can be obtained, and each state is corresponding to one known deviation value ε_j in the AMDM, i.e. $[\boldsymbol{X}_j, \varepsilon_j]$. The form of partial training data is shown in Table 5.

Table 5 indicates that the differences between orbit states obtained from different models are relatively small. Therefore, it is hard for a traditional statistical method to find out the relationship between satellite on-orbit state $\boldsymbol{X}_j$ and known deviation value ε_j. This is the main reason why this paper applies the typical methods in data mining to process and classify these large amounts of data.

TABLE 5. Partial training data examples.

ε_j	Δt (day)	a(km)	e	i(°)	Ω (°)	ω (°)	M(°)
-50%	0.301	6871.102	0.0025	97.565	286.288	94.707	229.007
-40%	0.600	6871.051	0.0025	97.563	286.395	93.301	72.578
-30%	0.300	6871.102	0.0025	97.565	286.088	94.701	227.745
-20%	0.600	6871.048	0.0025	97.563	286.395	93.299	73.216
-10%	0.500	6871.142	0.0025	97.561	286.293	94.098	243.763
0%	0.900	6871.174	0.0025	97.563	286.699	93.709	278.117
10%	0.800	6871.061	0.0025	97.565	286.597	93.410	87.899
20%	0.200	6871.072	0.0025	97.564	285.986	95.067	39.982
30%	0.300	6871.096	0.0025	97.565	286.088	94.703	228.378
40%	0.500	6871.135	0.0025	97.561	286.293	94.097	243.766
50%	0.600	6871.036	0.0025	97.563	286.395	93.298	73.220

In this section, the procedure for the application of data mining methods to recover the deviation of AMDM is as following: Firstly, four-fifths satellite on-orbit states are firstly regarded as the training data to obtain the classifiers in the guarantee of the data consistency. Then, the remaining one-fifth data are included to compare and evaluate the training results. It can reveal the generalization ability of the proposed methods. The classification model accuracy is defined respectively: in terms of RF and SVM, it is considered as a correct prediction when the classification prediction is identical to the artificial ones and the accuracy metric is scaled by the percentage of correct prediction; as for ANN, the accuracy metric is formulated by $|\varepsilon_p - \varepsilon_j| < 1 \times 10^{-3}$ where ε_p is deviation value predicted by ANN and 1×10^{-3} is the threshold due to 1×10^{-1} as a minimum step.

TABLE 6. Training parameter setting of RF.

Classification Model	Number of DT
RF	50

Three classification methods have been introduced in Section III, and the training data have been obtained from the above content. Some other parameter settings are tabulated in Tables 6-8 to complete the initialization of each classification method. The selection of parameters includes two aspects: 1) rough selection: according to the number of variables and the size of the data set, a reasonable parameter interval is determined through experience; 2) fine selection: by using the control variable method and constantly changing the single parameter value within its interval, the final choice is the value of the parameter with the highest model accuracy.

TABLE 7. Training parameter setting of ANN.

Classification Model	Hidden Layers	Number of Neurons*	Training Function
Feed-forward Backpropagation Network	5	20	TRAINLM
Adaption Learning Function	Max Fail	Min Gradient	Performance Function
LEARNGDM	10	1×10-9	Mean Square Error (MSE)

*: Except the last layer which is output layer, other 4 layers each have 20 neurons.

TABLE 8. Training parameter setting of SVM.

Classification Model	Kernel Function	Kernel Scale	Box Constraint Level	Multiclass Method
SVM	Quadratic	Automatic	1	One-vs-One

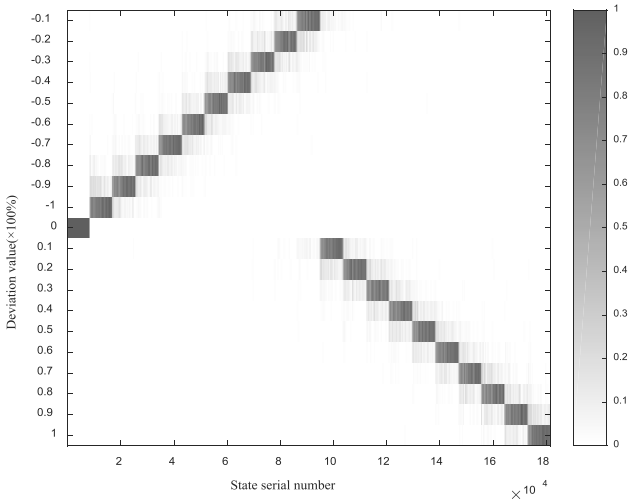

(a)

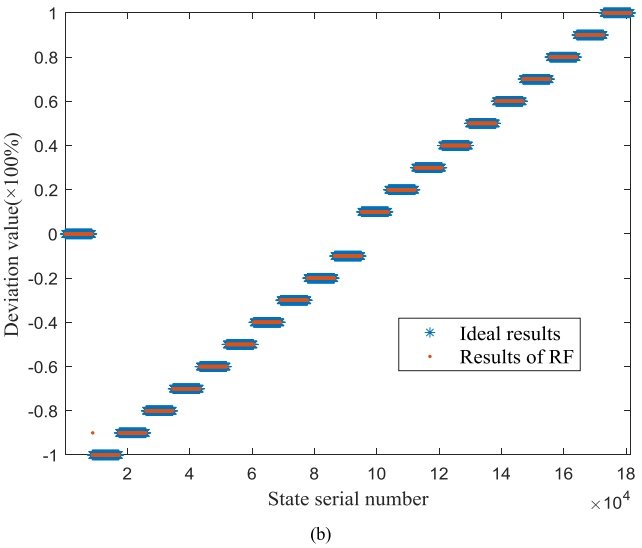

(b)

FIGURE 6. Results of RF: ideal results and classified ones are shown; a confusion matrix; b voting results of RF.

B. COMPARISON AND EVALUATION OF TRAINING RESULTS

The results of RF are shown in Figure 6, where x-axis means the serial number of each on-orbit state, and y-axis means the

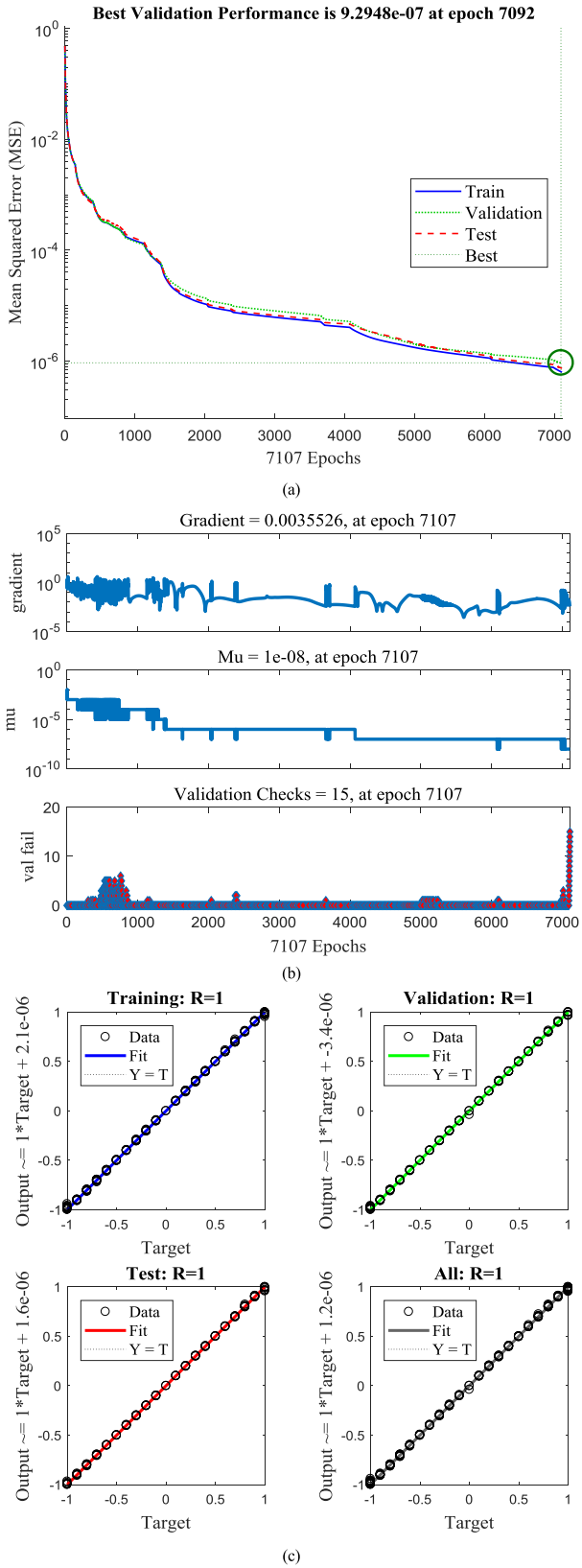

FIGURE 7. Training results of ANN: a change of MSE; b change of gradient, mu and validation fail; c results regression.

deviation value of this state predicted through RF. Because of the voting mechanism, the result in Figure 6b is obtained

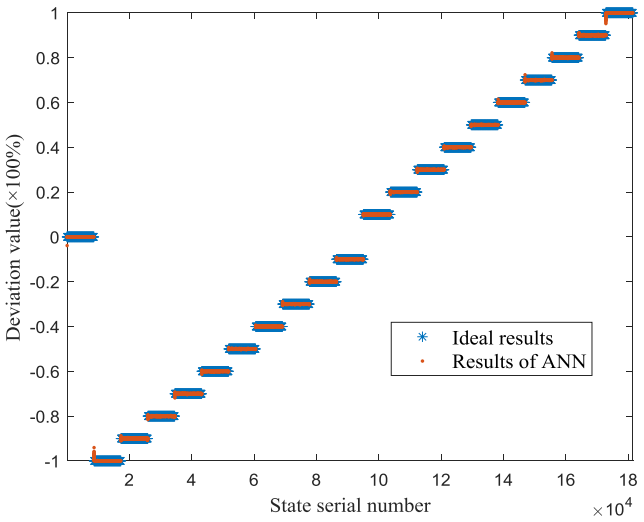

FIGURE 8. Classification results of ANN: ideal results and classified ones are shown.

through choosing the value which has the maximum probability in Figure 6a. It is obviously indicated from Figure 6a that the color is deeper, the probability is larger. Beneficial from the randomness and the voting mechanism of RF, the final accuracy of the classification is up to 99.99%. It should be noted that the accuracy is obtained by calculating the ratio of correct classification value.

Figure 7 gives the training process and results of ANN. Figure 7a shows that during 7107 iterations, ANN continuously adjusts the weight to reduce the value of performance function, i.e. MSE, gradually. The minimal value of MSE is 9.2948×10^{-7}. Figure 7b shows the evolvement rules of the gradient, mu (in TRAINLM) and validation fail during 7107 iterations. It also indicates that the validation fails in achieving its maximum value in the end and ANN stops its training process. Figure 7c presents the regression results where the x-axis means the known deviation value, while the y-axis means the predicted deviation value. If the small circles in Figure 7c are closer to the diagonal, the training results are better. Four subfigures, displaying "Training Set", "Validation Set", "Test Set", and "ALL Data" respectively, show different results of different data partitions.

Similar to Figure 6, Figure 8 shows the results of ANN. The accuracy of the results has better reduced compared with RF. It should be noted that after training, ANN can generate new classes for data (i.e. new deviation values which are different from the known values), which is more obvious when the prediction time is small. While the results of RF only show the original classes. This ability of ANN is called generalization ability referred to as the networks producing reasonable "new" outputs for inputs during training. As shown in Table 5, the training data are discrete. But the results of ANN are nearly linearly varying. Moreover, Figure 9 demonstrates the errors between ideal results and the ones of ANN which indicate the accuracy of ANN. It shows more clearly that early on-orbit states with shorter prediction time possess larger

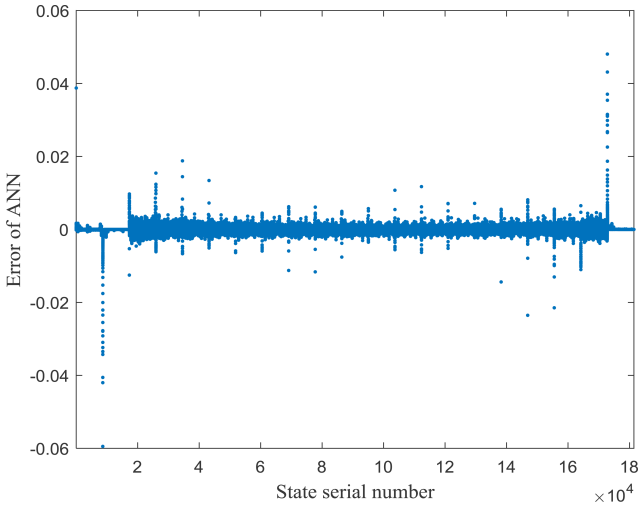

FIGURE 9. Prediction error of ANN: the error between ideal results and the ones of ANN.

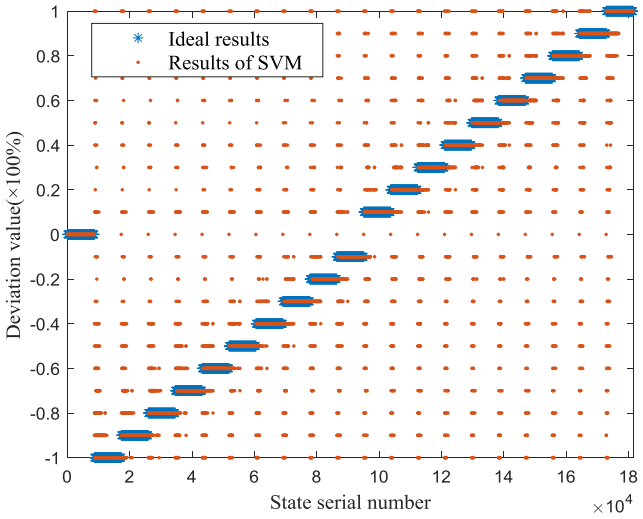

FIGURE 10. Classification results of SVM: ideal results and classified ones are shown.

error. With the increase of the prediction time, the prediction errors reduce gradually.

Figure 10 shows the classification results of SVM. The accuracy of SVM is only 71.90%. The similarity of ANN and SVM is that when the prediction time is small, the differences between different models are small, and the results may have larger errors. Moreover, the results of ANN only fluctuate within a certain range, while the results of SVM fluctuate within the whole domain discretely. Moreover, SVM and RF will not generate new classes which demonstrates that ANN possesses the best generalization ability.

The comparison of the three methods is tabulated in Table 9. It indicates clearly that RF owns the shortest training time and the highest accuracy. Considering the number of DT is 50, properly reducing the number may shorten training time and meanwhile not reduce the accuracy. On the other hand, the results of ANN and SVM are not ideal. As for these two

TABLE 9. Comparison of three classification methods.

Classification method	Training time(s)	Accuracy
RF	241.4342	99.99%
ANN	237937.0000	86.83%
SVM	65167.6274	71.90%

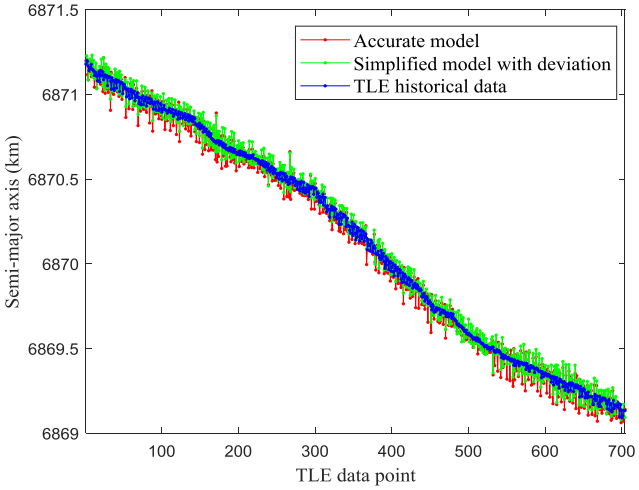

FIGURE 11. Change of semi-major axis: the accurate model is denoted by the red line, the simplified model with deviation is denoted by the green one, and historical TLE data are denoted by the blue one.

methods, the training data of on-orbit states and atmospheric deviation values used in this paper are hard to train. Notice that the training time of ANN and SVM is far beyond 200 times more than RF. Especially for ANN, this training method will occur overfitting and failure easily. This section chooses 1×10^{-3} as a calculation standard. When the calculation standard is lowered, such as 1×10^{-2}, the accuracy of ANN may achieve more than 95%.

IV. APPLICATION OF CLASSIFIERS IN IMPROVING THE ACCURACY OF ORBITAL PREDICTION

From the perspective of methodology, Section III investigates the feasibility of the three methods in recovering the known deviation ε_j in the AMDM under the simulation environment. However, Section III is conducted under a pure simulation environment. In this section of practical application, new training data and application data are firstly generated by using the two dynamical models and historical TLE data. Three classifiers are retrained and used to process the application data. After recovering the unknown deviation, the results are implemented to improve the AMDM in accurate dynamical model in terms of different classification methods respectively.

A. GENERATION OF NEW TRAINING AND APPLICATION DATA

For better understanding, this section uses the change of the semi-major axis to show the process of data generation, shown in Figure 11. The blue points mean the orbit states

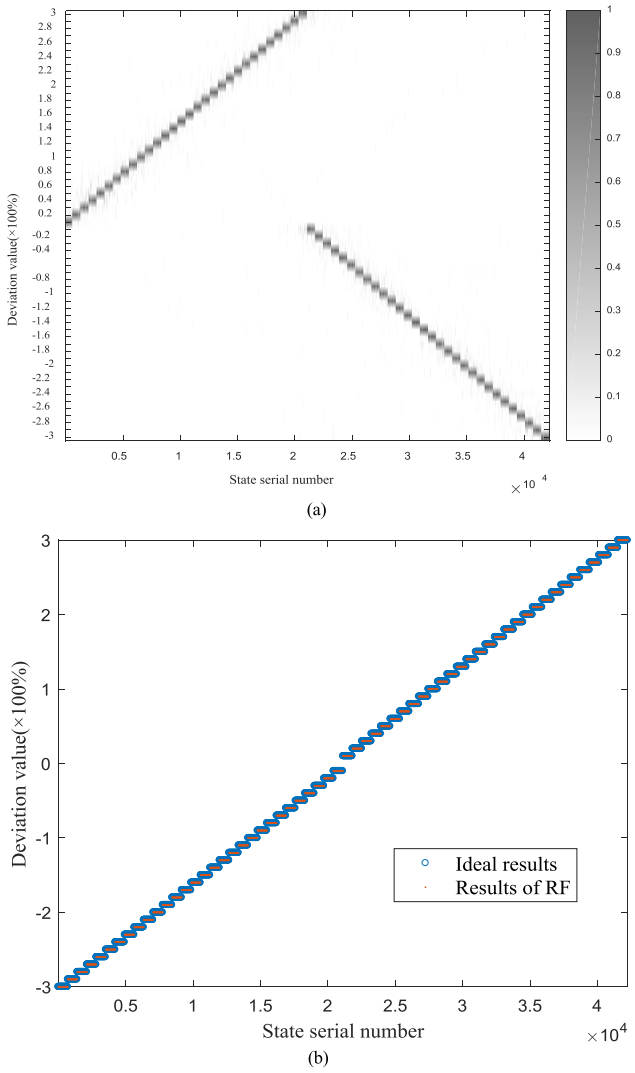

FIGURE 12. Results of RF: ideal results and classified ones are shown; a confusion matrix; b voting results of RF.

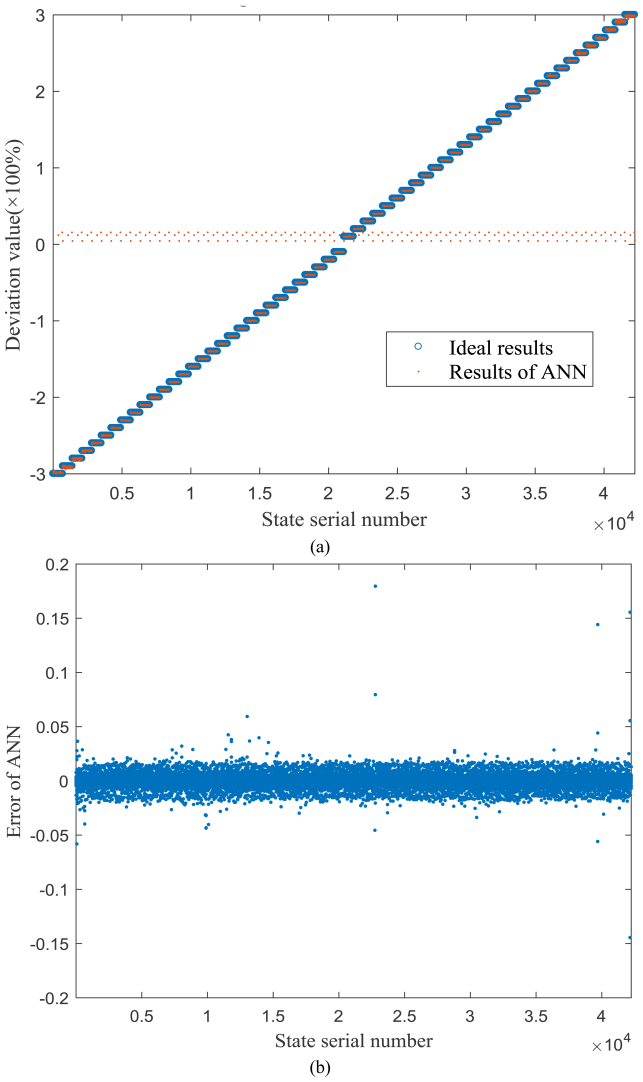

FIGURE 13. Retraining results of ANN: a classification results; b prediction errors.

calculated from historical TLE data. 704 TLE data points are chosen as the benchmark of simulation and there is no orbital maneuver among these points. The red points mean the orbit states calculated from the accurate dynamical model. The green points mean the orbit states calculated from the simplified model with deviation. It should be noted that the deviation value ε_s in Figure 11 is equal to 300%. In order to calculate the differences between historical TLE data and different dynamical models to generate new training and application data, the prediction interval is the interval of adjacent TLE data points.

Figure 11 indicates that there are considerable prediction errors between historical TLE data and the dynamical models. Similar to Section III, three types of orbit states are recorded at every epoch corresponding to the accurate model $\boldsymbol{X}_a$, the simplified model with deviation $\boldsymbol{X}_s$ and historical TLE data $\boldsymbol{X}_t$. The differences between $\boldsymbol{X}_a$ and $\boldsymbol{X}_s$ can be regarded as new training data, while the differences between $\boldsymbol{X}_a$ and $\boldsymbol{X}_t$ can be regarded as application data. The forms of partial training and application data are shown in Tables 10 and 11, respectively. Based on the actual engineering experience, the range of known deviation values in AMDM is extended to $[-300\%, 300\%]$ in this section. It is worth mentioning that the deviation values which are smaller than -100% mean that atmosphere causes a larger lift force than the drag force due to the satellite's attitude.

B. RETRAINING RESULTS OF NEW CLASSIFIERS

Three methods are used to learn new training data and generate new classifiers. Some different settings are listed as follows to adapt to new training data and reduce computational burden: 1) the number of DT in RF reduces to 25; 2) the number of neurons in each layer increases to 30. The other parameter settings are in accordance with Tables 6-8. Retraining results are shown in Figures 12-14. It can be seen that both RF and SVM give results with high accuracy, while there are some discrete points in ANN results.

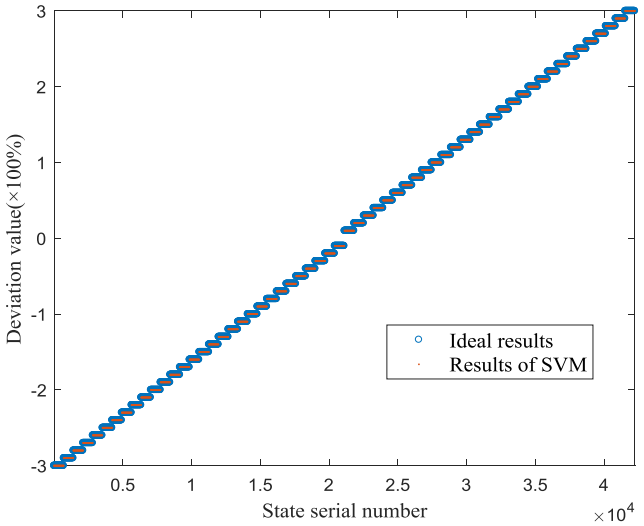

FIGURE 14. Retraining Results of SVM: ideal results and classified ones are shown.

TABLE 10. Partial new training data examples.

ε_j (%)	Δt (day)	a (km)	e	i (°)	Ω (°)	ω (°)	M (°)
-300	0.3225	6871.1835	0.0025	97.5640	286.1095	94.6685	349.1779
-270	0.3225	6871.1808	0.0025	97.5640	286.1095	94.6686	349.1784
-230	0.2628	6871.2225	0.0025	97.5585	286.3770	93.4320	350.8553
-180	0.4001	6871.1756	0.0024	97.5594	286.7760	93.9994	23.1031
-60	0.3821	6871.0597	0.0025	97.5635	287.1628	92.9055	318.1787
30	0.1332	6871.1842	0.0025	97.5583	287.2966	92.5408	328.5835
110	0.5352	6871.1466	0.0025	97.5606	287.8363	91.9872	21.9665
170	0.3243	6871.1227	0.0025	97.5633	288.1619	91.4528	359.5529
220	0.3292	6871.0532	0.0025	97.5634	289.1594	89.7870	28.9062
260	0.3261	6871.0612	0.0025	97.5566	289.8199	88.9329	28.4148
300	0.3303	6871.1279	0.0025	97.5608	290.4870	86.4204	43.4925

TABLE 11. Partial application data examples.

Δt (day)	a(km)	e	i(°)	Ω (°)	ω (°)	M(°)
0.3225	6871.1993	0.0025	97.5639	286.1093	94.9526	348.8834
0.2628	6871.2059	0.0025	97.5588	286.3771	92.9178	351.3704
0.4001	6871.1165	0.0024	97.5593	286.7760	94.4643	22.6408
0.3821	6871.0855	0.0025	97.5639	287.1625	93.3412	317.7268
0.1332	6871.1713	0.0025	97.5581	287.2969	92.1457	328.9794
0.5352	6871.1332	0.0025	97.5611	287.8362	92.2625	21.6711
0.3243	6871.1961	0.0025	97.5623	288.1611	91.8699	359.1118
0.3237	6871.1045	0.0025	97.5618	288.4908	89.4844	335.2834
0.3375	6871.1314	0.0024	97.5573	288.8264	91.2313	23.3758
0.3292	6871.1615	0.0025	97.5623	289.1588	90.1748	28.4940
0.3306	6871.1308	0.0025	97.5612	289.4950	87.9460	42.5073

TABLE 12. Statistic error values of each model and method.

Statistic Values	Training Model	Accurate Model	Improved Accurate Model		
			RF	ANN	SVM
a (km)	0.0328	0.0478	0.0395	0.0480	0.0479
e (10^{-5})	1.2575	2.7649	2.7642	2.7649	2.7646
i (°)	0.0004	0.0027	0.0027	0.0027	0.0027
Ω (°)	0.0003	0.0030	0.0030	0.0030	0.0030
ω (°)	0.8020	1.7636	1.7629	1.7635	1.7632
M (°)	0.8030	1.7602	1.7604	1.7600	1.7598

The errors of ANN are also increased compared with the ones in Section III. One of the reasons is the larger data set and ANN possesses the generalization ability. Obviously, RF still possesses the highest accuracy.

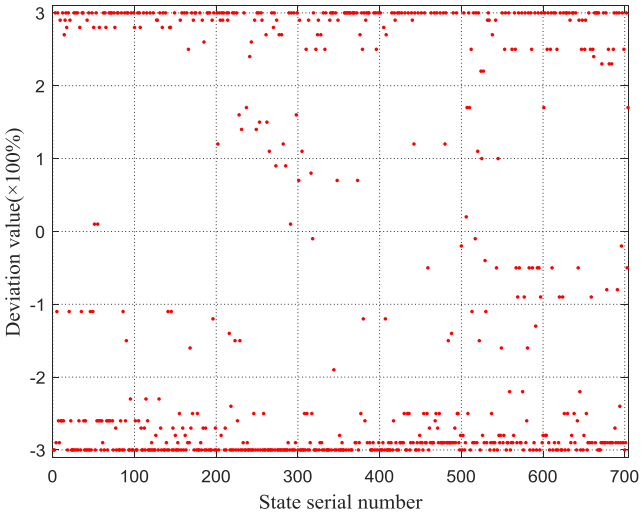

FIGURE 15. Application results of RF: deviation is denoted by red points.

TABLE 13. Performance indicator of each method.

Classification method	DMAE (m)
RF	5.9739
ANN	0.8930
SVM	0.8082

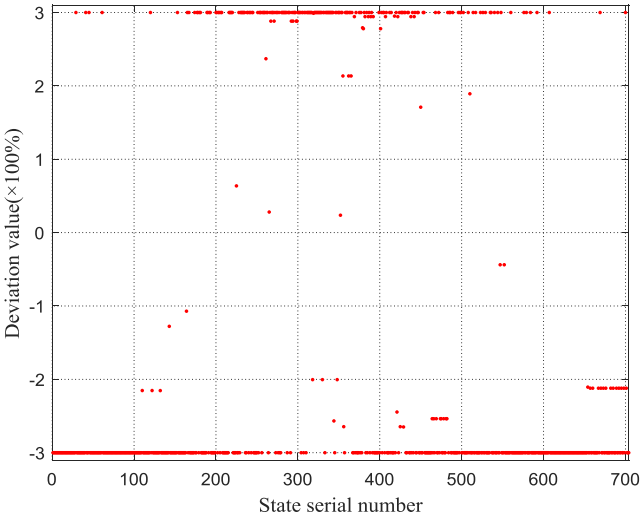

FIGURE 16. Application results of ANN: deviation is denoted by red points.

C. APPLICATION ANALYSIS OF CLASSIFIERS

Three retrained classifiers are used to process the application data, respectively. Figures 15-17 show the application results and comparison of the application results of different methods, respectively. It is obvious that the predicted deviation values between the accurate model and historical TLE data range from -300% to 300%. Owing to the high accuracy, RF can recover relatively small deviation, while ANN and SVM can only recover partial values. Different from RF and ANN, the results of SVM present a type of stepped distribution.

The validity and accuracy of each method are not intuitive in Figures 15-17 which only present the recovering results of deviation values. It is necessary to prove the effects of

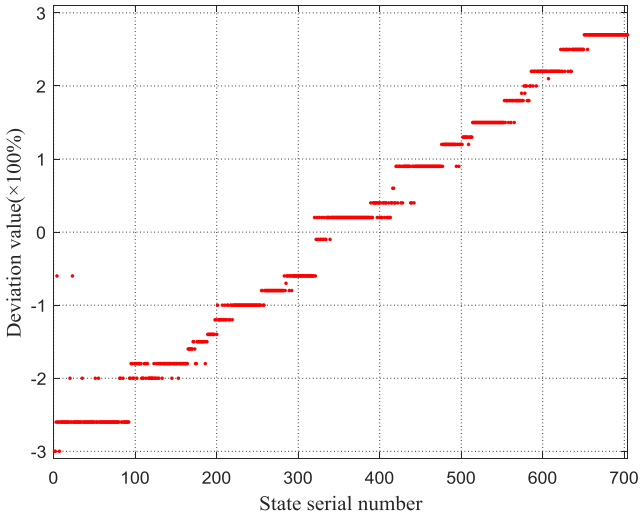

FIGURE 17. Application results of SVM: deviation is denoted by red points.

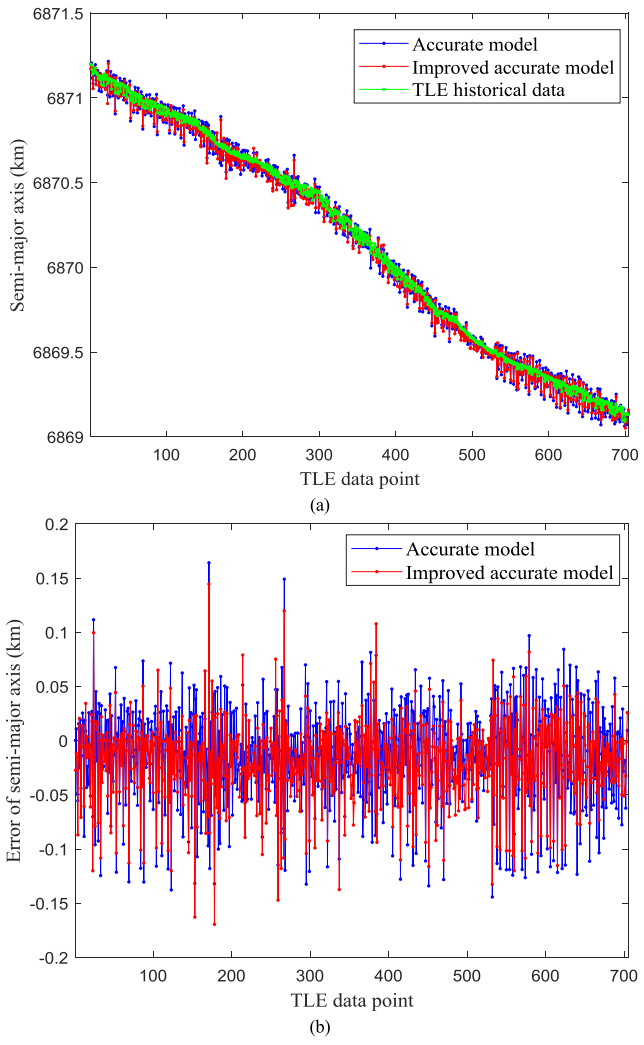

FIGURE 18. Improvement results of RF: a change of semi-major axis; b errors of semi-major axis.

the improvement in a realistic orbit prediction application. Therefore, the deviation errors in terms of different classification methods are added to the accurate model to improve the

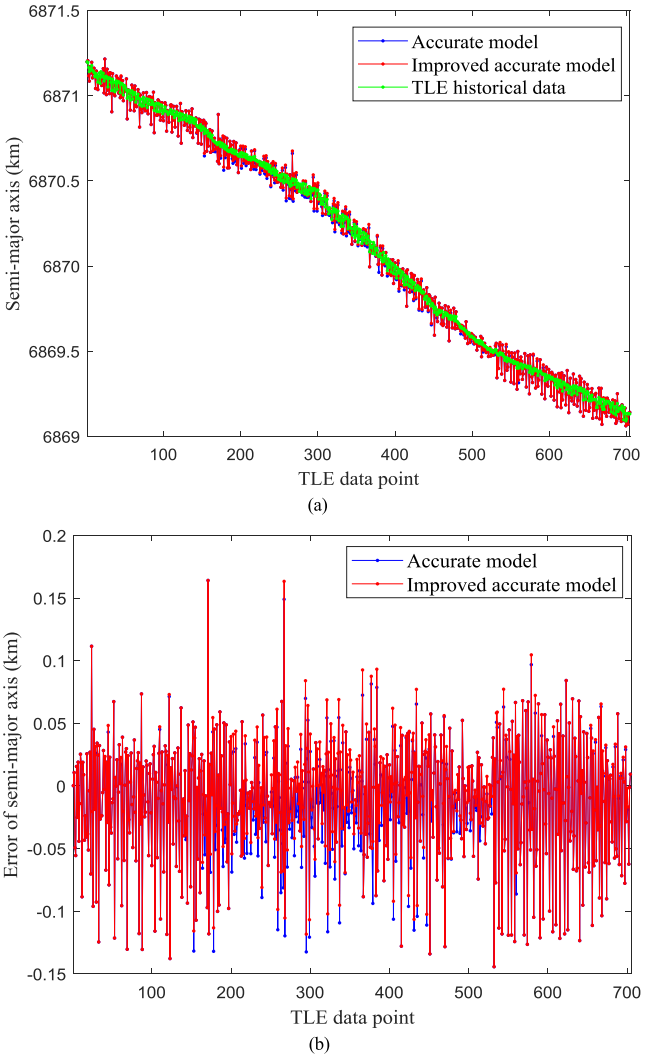

FIGURE 19. Improvement results of ANN: a change of semi-major axis; b errors of semi-major axis.

AMDM respectively, namely the improved accurate model. Figures 18a-20a are the orbital prediction results using the improved accurate model corresponding to each method. Figures 18b-20b show the errors caused by the accurate models and improved accurate ones based on historical TLE data. Because of the uneven recording intervals and the small sample size of the TLE data used here, i.e. 2-4 TLE data samples a day released by NOARD, it can reveal the seasonal short-term variation instead of diurnal instantaneous one.

In order to qualify the improvement in orbit prediction of the three methods, the statistic error values of each model and method are given in Table 12. Standard deviations of the orbital element errors are regarded to scale the relative dispersion of AMDM errors. The second column is denoted the training model errors, i.e. the differences between $\boldsymbol{X}_a$ and $\boldsymbol{X}_s$. The third is the statistic value of application data. The others are the ones of improved accurate model errors using different classification methods. What's more, this paper chooses a performance indicator, Difference of Mean Absolute Error (DMAE) which can be calculated through the

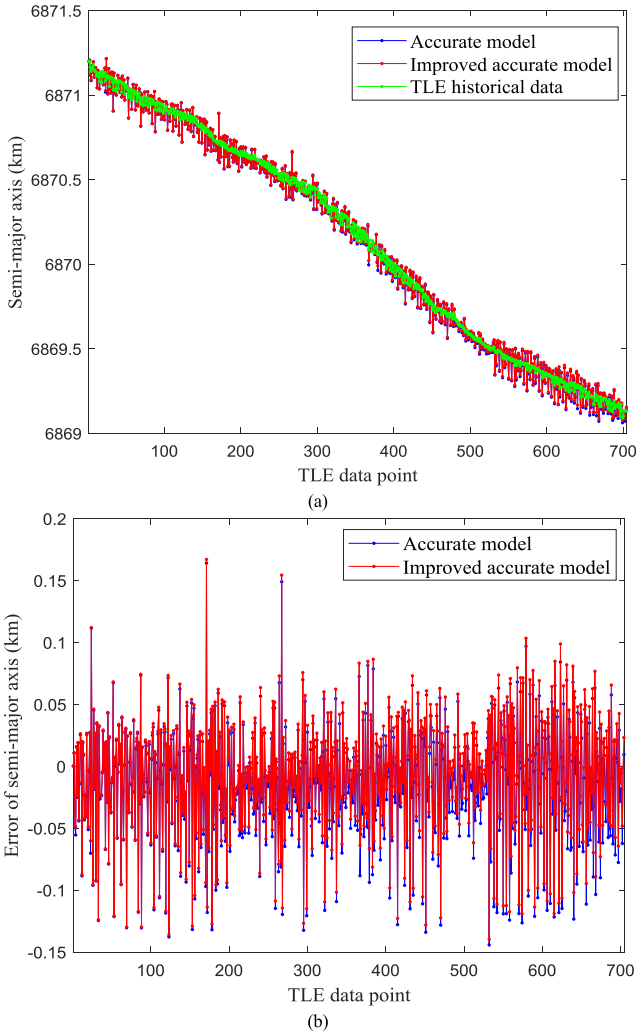

FIGURE 20. Improvement results of SVM: a change of semi-major axis; b errors of semi-major axis.

following Equation (12):

$$\mathrm{DMAE} = mean\left(|a_a - a_t|\right) - mean\left(\left|a_{imp} - a_t\right|\right) \quad (12)$$

where $mean(\cdot)$ is the function for calculating the average value. a_a is the semi-major axis calculated by the original accurate model. a_t is the semi-major axis calculated by historical TLE data. a_{imp} is the semi-major axis calculated by the improved accurate model. As shown in Tables 12 and 13, the three classification methods in this paper can improve part of atmospheric density models inside the accessible data. Among the three improved accurate models, RF shows the greatest accuracy, which is analogous to the DMAE results.

V. CONCLUSION

This paper focuses on the orbital prediction of TIANHUI and data mining technology. Firstly, the mathematic models of the space environment are built, and two orbital dynamical models are proposed based on the detailed perturbations. The accurate model is used to simulate the ''actual'' space environment, while the simplified one with the known deviation is regarded as the basis of training data. Secondly, this paper introduces three classification methods, including their theories and characteristics. After the above two parts, this paper unfolds from two major aspects: methodology and practical application. In the stage of methodology, the two orbital dynamical models are used to generate training data starting from one specific epoch. And the three classification methods are used to train the data. The training results show that data mining technology can predict the known deviation values in AMDM. Especially for RF, the accuracy of RF can achieve 99.99%, while the ones of ANN and SVM are only 86.83% and 71.90% respectively. In the stage of practical application, new training data and application data are generated based on historical TLE data. In terms of the new training data, three classifiers are retrained and used to figure out the errors. The application results show that all the methods can recover the unknown deviation of AMDM in the accurate model. Using the improved accurate model to conduct orbital prediction, the three methods show certain capabilities of improving orbital prediction, of which RF still possesses the best performance which maximum DMAE.

This paper provides novel thoughts and data mining methods for orbital prediction. The proposed methods improve part of atmospheric density models inside the accessible data based on the point-to-point historical TLE data, instead of replacing the traditional models. Its dependence on data makes it more updated. Its correction of empirical atmospheric density model offers a more reliable and accurate way of orbital propagation and extends the validity of atmospheric density model. Combining with popular data mining technology, this paper explores the application of the data mining method in traditional aerospace engineering and provides favorable reference. In the future work, based on more accurate orbital information, such as GPS post-processing data, a systematic two-level correction will be proposed: the first level is to improve the atmospheric density on specified heights from TLE data of limited LEO and the second one is to mine all the height span of atmospheric density from the results achieved in the first level. The correction of full atmospheric density model varying instantaneously as well as with more detailed perturbations are worth investigating.

REFERENCES

[1] I. H. Witten, E. Frank, and M. A. Hall, ''What's it all about,'' in *Data Mining: Practical Machine Learning Tools and Techniques*, 3rd ed. Cambridge, MA, USA: Morgan Kaufmann, 2011, p. 338.

[2] L. Self, ''Use of data mining on satellite data bases for knowledge extraction,'' presented at the 13th Int. Florida Artif. Intell. Res. Soc. Conf., Orlando, FL, USA, May 2000.

[3] T.-C. Fu, ''A review on time series data mining,'' *Eng. Appl. Artif. Intell.*, vol. 24, no. 1, pp. 164–181, Feb. 2011, doi: 10.1016/J.ENGAPPAI.2010.09.007.

[4] F. M. Bianchi, A. Rizzi, A. Sadeghian, and C. Moiso, ''Identifying user habits through data mining on call data records,'' *Eng. Appl. Artif. Intell.*, vol. 54, pp. 49–61, Sep. 2016, doi: 10.1016/j.engappai.2016.05.007.

[5] N. Pillay, R. Qu, D. Srinivasan, B. Hammer, and K. Sorensen, ''Automated design of machine learning and search algorithms [guest editorial],'' *IEEE Comput. Intell. Mag.*, vol. 13, no. 2, pp. 16–17, May 2018, doi: 10.1109/mci.2018.2806988.

[6] H.-J. Li and L. Wang, "Multi-scale asynchronous belief percolation model on multiplex networks," *New J. Phys.*, vol. 21, no. 1, Jan. 2019, Art. no. 015005, doi: 10.1088/1367-2630/aaf775.

[7] H.-J. Li, Z. Bu, Z. Wang, J. Cao, and Y. Shi, "Enhance the performance of network computation by a tunable weighting strategy," *IEEE Trans. Emerg. Topics Comput. Intell.*, vol. 2, no. 3, pp. 214–223, Jun. 2018, doi: 10.1109/TETCI.2018.2829906.

[8] H.-J. Li, Z. Bu, Z. Wang, and J. Cao, "Dynamical clustering in electronic commerce systems via optimization and leadership expansion," *IEEE Trans. Ind. Informat.*, vol. 16, no. 8, pp. 5327–5334, Aug. 2020, doi: 10.1109/TII.2019.2960835.

[9] M.-S. Chen, J. Han, and P. S. Yu, "Data mining: An overview from a database perspective," *IEEE Trans. Knowl. Data Eng.*, vol. 8, no. 6, pp. 866–883, Dec. 1996, doi: 10.1109/69.553155.

[10] S. Tanner, C. Stein, and S. J. Graves, "On-board data mining," in *Scientific Data Mining and Knowledge Discovery*. Berlin, Germany: Springer, 2009, pp. 345–376, doi: 10.1007/978-3-642-02788-8_13.

[11] C. Sánchez-Sánchez, D. Izzo, and D. Hennes, "Learning the optimal state-feedback using deep networks," presented at the IEEE Symp. Ser. Comput. Intell. (SSCI), Athens, Greece, 2016, doi: 10.1109/SSCI.2016.7850105.

[12] D. Hennes, D. Izzo, and D. Landau, "Fast approximators for optimal low-thrust hops between main belt asteroids," presented at the IEEE Symp. Ser. Comput. Intell. (SSCI), Athens, Greece, 2016, doi: 10.1109/ssci.2016.7850107.

[13] D. Li, S. Wang, D. Li, and X. Wang, "Theories and technologies of spatial data mining and knowledge discovery," *Geometrics Inf. Sci. Wuhan Univ.*, vol. 27, no. 3, pp. 221–223, 2002, doi: 10.1080/12265080208422884.

[14] H. Gong, W. Zhao, and J. Li, "The technological framework of data mining from the polygenetic remotely sensed data," *J. Image Graph.*, vol. 10, no. 5, pp. 620–623, 2005.

[15] H. Peng and X. Bai, "Recovering area-to-mass ratio of resident space objects through data mining," *Acta Astron.*, vol. 142, pp. 75–86, Jan. 2018, doi: 10.1016/j.actaastro.2017.09.030.

[16] H. Peng and X. Bai, "Improving orbit prediction accuracy through supervised machine learning," *Adv. Space Res.*, vol. 61, no. 10, pp. 2628–2646, May 2018, doi: 10.1016/j.asr.2018.03.001.

[17] H. Peng and X. Bai, "Exploring capability of support vector machine for improving satellite orbit prediction accuracy," *J. Aerosp. Inf. Syst.*, vol. 15, no. 6, pp. 366–381, Jun. 2018, doi: 10.2514/1.i010616.

[18] X. Hu, Z. Li-Juan, and Y. Wang, "The Analysis of Data Mining Strategy in Fault Detection and Diagnosis of the Liquid Rocket Engine," *J. Nat. Univ. Defense Technol.*, vol. 27, no. 3, pp. 1–5, 2005, doi: 10.3969/j.issn.1001-2486.2005.03.001.

[19] Y. Xu and D. Pi, "Method to mine satellite abnormal patterns," *J. Chin. Comput. Syst.*, vol. 36., no. 9, pp. 1988–1992, 2015, doi: 10.3969/j.issn.1000-1220.2015.09.014.

[20] G. Zhao and Y. Li, "Spacecraft fault diagnosis method based on time series Data Mining," *J. Spacecraft TT C Technol.*, vol. 29, no. 3, pp. 1–5, 2010, doi: CNKI:SUN:FXCK.0.2010-03-002.

[21] X. Bai, C. Liao, X. Pan, and M. Xu, "Mining two-line element data to detect orbital maneuver for satellite," *IEEE Access*, vol. 7, pp. 129537–129550, 2019, doi: 10.1109/access.2019.2940248.

[22] T. S. Kelso, F. Hoots, and R. Roehrich, "Models for propagation of NORAD element sets," Spacetrack, Exton, PA, USA, Tech. Rep. 3, Dec. 1988.

[23] E. Kahr, O. Montenbruck, and K. P. G. O'Keefe, "Estimation and analysis of two-line elements for small satellites," *J. Spacecraft Rockets*, vol. 50, no. 2, pp. 433–439, Mar. 2013.

[24] D. Li, J. Liu, and Y. Zhang, "TLE accuracy analysis and conjunction prediction," *Chin. J. Space Sci.*, vol. 32, no. 3, pp. 398–404, 2012, doi: 10.11728/cjss2012.03.398.

[25] R. E. Shanklin, T. Lee, M. Samii, M. K. Mallick, and J. O. Cappellari, "Comparative studies of atmospheric density models used for Earth satellite orbit estimation," *J. Guid., Control, Dyn.*, vol. 7, no. 2, pp. 235–237, Mar. 1984, doi: 10.2514/3.8572.

[26] L. G. Jacchia, "Static diffusion models of the upper atmosphere with empirical temperature profiles," *Smithsonian Contrib. Astrophys.*, vol. 8, no. 9, pp. 213–257, 1965, doi: 10.5479/si.00810231.8-9.213.

[27] A. E. Hedin, "MSIS-86 thermospheric model," *J. Geophys. Res.*, vol. 92, no. A5, p. 4649, 1987, doi: 10.1029/ja092ia05p04649.

[28] S. Bruinsma, G. Thuillier, and F. Barlier, "The DTM-2000 empirical thermosphere model with new data assimilation and constraints at lower boundary: Accuracy and properties," *J. Atmos. Solar-Terr. Phys.*, vol. 65, no. 9, pp. 1053–1070, Jun. 2003, doi: 10.1016/s1364-6826(03)00137-8.

[29] B. R. Bowman, W. K. Tobiska, F. A. Marcos, and C. Valladares, "The JB2006 empirical thermospheric density model," *J. Atmos. Solar-Terr. Phys.*, vol. 70, no. 5, pp. 774–793, Mar. 2008, doi: 10.1016/j.jastp.2007.10.002.

[30] B. Bowman, W. K. Tobiska, F. Marcos, C. Huang, C. Lin, and W. Burke, "A new empirical thermospheric density model JB2008 using new solar and geomagnetic indices," presented at the AIAA/AAS Astrodyn. Specialist Conf. Exhib., Honolulu, HI, USA, Aug. 21, 2008, doi: 10.2514/6.2008-6438.

[31] P. Cefola, I. I. Volkov, and V. V. Suevalov, "Description of the Russian upper atmosphere density model GOST-2004," presented at the in 37th COSPAR Sci. Assem., Montreal, QC, Canada, Jul. 2008, doi: 10.2514/6.1995-554.

[32] J. T. Emmert, J. M. Picone, and R. R. Meier, "Thermospheric global average density trends, 1967–2007, derived from orbits of 5000 near-Earth objects," *Geophys. Res. Lett.*, vol. 35, no. 5, pp. 1967–2007, Mar. 2008, doi: 10.1029/2007GL032809.

[33] R. G. Melton, "Fundamentals of astrodynamics and applications," *J. Guid., Control, Dyn.*, vol. 21, no. 4, p. 672, Jul. 1998, doi: 10.2514/2.4291.

[34] E. Doornbos, H. Klinkrad, and P. Visser, "Atmospheric density calibration using satellite drag observations," *Adv. Space Res.*, vol. 36, no. 3, pp. 515–521, Jan. 2005, doi: 10.1016/j.asr.2005.02.009.

[35] E. Doornbos, H. Klinkrad, and P. Visser, "Use of two-line element data for thermosphere neutral density model calibration," *Adv. Space Res.*, vol. 41, no. 7, pp. 1115–1122, Jan. 2008, doi: 10.1016/j.asr.2006.12.025.

[36] J. Chen, J. Du, and J. Sang, "Improved orbit prediction of LEO objects with calibrated atmospheric mass density model," *J. Spatial Sci.*, vol. 64, no. 1, pp. 97–110, Sep. 2017, doi: 10.1080/14498596.2017.1371089.

[37] G. Beutler, "High order oblateness perturbation characteristics," in *Methods of Celestial Mechanics: Application to Planetary System, Geodynamics and Satellite Geodesy*, vol. 2, 1st ed. Berlin, Germany: Springer, 2005, pp. 142–154.

[38] O. Montenbruck, E. Gill, and F. Lutze, "Satellite orbits: Models, methods, and applications," *Appl. Mech. Rev.*, vol. 55, no. 2, p. B27, 2002, doi: 10.1115/1.1451162.

[39] S. C. Kenyon, "The Development by the national imagery and mapping agency of a global surface gravity anomaly database for the EGM96 geopotential model and future applications," in *Proc. Int. Assoc. Geodesy Symposia*, 1998, pp. 99–104, doi: 10.1007/978-3-642-72245-5_12.

[40] X. Jia, M. Xu, X. Pan, and X. Mao, "Eclipse prediction algorithms for low-earth-orbiting satellites," *IEEE Trans. Aerosp. Electron. Syst.*, vol. 53, no. 6, pp. 2963–2975, Dec. 2017, doi: 10.1109/taes.2017.2722518.

[41] M. Zijlstra, S. Theil, and S. Scheithauer, "Model for short-term atmospheric density variations," in *Earth Observation With CHAMP: Results From Three Years in Orbit*. Berlin, Germany: Springer, 2005, pp. 489–494, doi: 10.1007/3-540-26800-6_77.

XUE BAI received the B.S. degree in spacecraft design and engineering from the School of Astronautics, Beihang University, Beijing, China, where she is currently pursuing the M.S. degree. Her research interests include formation flying, circular restricted three-body problem, and orbital big data mining.

CHUAN LIAO received the B.S. degree from the School of Aerospace Engineering, Beijing Institute of Technology, Beijing, China, in 2016, and the M.S. degree in aerospace engineering from Beihang University, Beijing, in 2019. He is currently working with the No. 10 Research Institute, China Electronics Technology Group Corporation, Chengdu, China. His research interests include spacecraft orbital dynamics and control, orbital big data mining, and inversion.

MING XU received the B.S. and Ph.D. degrees in aerospace engineering from Beihang University, Beijing, China, in 2003 and 2008, respectively. He was an Engineer in orbital design and operation with DFH Satellite Company Ltd., China Academy of Space Technology, Beijing, in 2010. He joined Beihang University, as an Assistant Professor, where he was promoted as an Associate Professor, in 2012. He has published 50 publications in journals, books, and proceedings. His current research interests include applications of dynamical systems theory into astrodynamics and orbital control. He received the National Top 100 Excellent Doctoral Dissertation Award Nomination, in 2010, and the Third Class Prizes of the National Defense Technology Invention Award, in 2016. He serves as an Associate Editor for the journals of *Astrodynamics* and *Advances in Aircraft and Spacecraft Science*.

YARU ZHENG received the M.S. degree in aerospace engineering from Beihang University, Beijing, China, in 2020. Her research interests include vehicle trajectory control and inertial navigation.